The International Archives of the Photogrammetry, Remote Sensing and Spatial Information Sciences, Volume XLVIII-2/W3-2023
ISPRS Intl. Workshop "Photogrammetric and computer vision techniques for environmental and infraStructure monitoring, Biometrics and Biomedicine"
PSBB23, 24–26 April 2023, Moscow, Russia

# ACCURATE CELL SEGMENTATION IN BLOOD SMEAR IMAGES BASED ON COLOR ANALYSIS AND CNN MODELS

N. Nishchhal[1], M. Favorskaya[1,*]

[1] Reshetnev Siberian State University of Science and Technology, Institute of Informatics and Telecommunications, 31, Krasnoyarsky Rabochy ave., Krasnoyarsk, 660037 Russian Federation - nishchhalkmr12@gmail.com, favorskaya@sibsau.ru

Commission II, WG II/8

**KEY WORDS:** Red Blood Cell, White Blood Cell, Color Space, Convolutional Neural Network, Segmentation.

**ABSTRACT:**

Nowadays, automated blood cell evaluation play a major role in the classification and diagnosis of diseases. Despite the many possible ways to segment blood cells, the recognition efficiency remains insufficient, especially when different cell types overlap. Also, one should not forget about the cells structure complexity. Image segmentation and image classification are the main stages of this problem. At the same time, segmentation of blood smear images is considered the most important stage in automated disease detection systems. Often cell segmentation in blood smear images is performed as a separate mapping for white blood cells and red blood cells. We propose another problem statement that uses the capabilities of supervised and unsupervised CNNs for the semantic segmentation of objects of different sizes and shapes. CNN has encoder-decoder architecture and builds a pseudo-color map. We tested several CNN models using different color spaces converting initial images from RGB to Lab, HSV and CMYK color spaces and obtained promising experimental results for several microscopic datasets such as CellaVision DM96, All-IDB and Blood Cell Detection.

## 1. INTRODUCTION

Hematology is a field of medicine that focuses on the study of the blood, and medical image processing holds a prominent position in this field. A vital hematological test frequently requested by medical practitioners to assess health is the complete blood cell (CBC) analysis, which includes cell segmentation, classification and counting. Red blood cells (RBCs), white blood cells (WBCs), and platelets are the three primary cell types that makeup blood. The majority of blood cells (around 40–45%) are RBCs, sometimes referred to as erythrocytes, which are the most prevalent form of a blood cell. Blood contains a large number of platelets, also known as thrombocytes. WBCs referred to as leukocytes, make up only 1% of all blood cells. The quantity of RBCs has an impact on how much oxygen is delivered to our bodily tissues by RBCs. Platelets aid in blood coagulation, whereas WBCs fight off infections.

Evaluation of hematologic disorders requires identification and description of the patient's blood. For the detection of disorders like anemia, leukemia, cancer, and other infectious diseases in pathological tests, the number of erythrocytes (red blood cells), leukocytes (white blood cells), platelets, and other blood cells are crucial. The majority of automated blood cell analysis systems are divided into three major phases: blood cell image segmentation, feature extraction, and blood cell classification. The segmentation of complex and varying shapes, as well as overlapping cells, is the most difficult phase of automation.

WBC segmentation is an important component of the CBC analysis system, and the results have a direct impact on cell recognition accuracy. Eosinophils, basophils, monocytes, leukocytes, and neutrophils are the five types of white blood cells. The first three are granular, while the last two are non-granular. The nonlinear optical method proved ineffective in distinguishing these types.

Unsupervised methods for WBC segmentation include image thresholding, image clustering, and edge detection, and are focused on features such as color, shape, and brightness. Image thresholding methods typically employ image features to calculate a threshold that is then employed to separate image pixels into object pixels and background pixels. They typically achieve satisfactory high contrast segmentation of WBC nuclei but fail to accomplish satisfactory low contrast segmentation of WBC cytoplasm.

A segmentation problem is regarded as a clustering algorithm by unsupervised methods. These methods typically extract image features before using them to classify image pixels. However, they are having difficulty with classification accuracy. Due to their limited image representation capability, traditional classifiers struggle to achieve high classification precision on large-scale image datasets. Currently, many deep learning models have been developed to improve segmentation results (Lu et al., 2021; Davamani et al., 2022; Dhalla et al., 2023).

In this paper, we propose, cell segmentation in blood smear images based on color analysis and encoder-decoder CNN models. The color intensity of blood smeared images taken with various light microscopes may differ slightly due to differences in image acquisition process conditions. Lighting conditions and the various devices used to collect samples are among the issues that must be addressed because it is critical to standardize the image's intensity in the system.

* Corresponding author

The paper is structured as follows. A brief review of related work is presented in Section 2. Section 3 describes materials and methods for color space correction and CNN-based segmentation. Section 4 contains the experimental results. Section 5 concludes the paper.

## 2. RELATED WORK

Traditional image segmentation methods include a wide variety of algorithms, which are classified as rule-based (thresholding-based segmentation, color-based segmentation, region-based segmentation, clustering-based segmentation, watershed segmentation, supervised segmentation methods, frequency domain methods, and so on) and deformable model-based (segmentation using active contours and level-set methods). They are presented in the literature published in 1980-2010 and discussed in detail in some surveys (Saraswath and Arya, 2014; Rodellar et al., 2018). The main challenges for these methods are noise removal with smoothing, Wiener filter, etc., as well as edge enhancement with morphological analysis, discrete curvelet transform, etc. Currently, these methods remain in the area of interest for creating hybrid approaches to the blood cell segmentation and classification. Adaptive cell segmentation using an improved fuzzy c-means algorithm was proposed in (Davamani et al., 2022), followed by an enhanced hybrid learning model with the help of long-short term memory and neural network classifiers.

Cell segmentation in blood smear image has different problem statements. There are a few publications on RBC segmentation, mostly based on color analysis. Many publications examine and develop methods for the WBC segmentation as a complex problem. At the same time, platelet segmentation is of no interest other than platelet counting (Shahzad et al., 2020; Drałus et al., 2021). Cell segmentation is usually performed in different color spaces in order to obtain separate WBCs and RBCs segmentation maps (Cao et al., 2018).

In recent years, deep convolution neural networks have become the SOTA of supervised image segmentation, demonstrating remarkable performance for medical image segmentation (Guo et al., 2019). The CNN encoder–decoder architectures can extract more contextual information, and most CNN segmentation models use this approach instead of representing the segmentation task as a classification task. The encoder, consisting of convolution operations, extracts optimal features, and the decoder restores the image resolution using interpolation methods or transposed convolutions. Typically, all the output feature maps from the encoder layers are associated with decoder layers to optimize the segmentation results in the form of a final output image. Such models show superiority in multi-scale feature detection compared to hand-crafted feature models.

The encoder can consist of some pre-defined networks. Let us list the commonly used models for semantic segmentation of medical images, among which are VGG (Simonyan and Zisserman, 2015), ResNet (He et al., 2016), SegNet (Tran et al., 2018), U-Net (Olaf et al., 2015; Kadry et al., 2022), U-Net++ (Lu et al., 2021), and DeepLabV3+ (Reena and Ameer, 2021). Recently, sophisticated models have been developed in this scope. A contour proposal network for instance segmentation that detects the possible overlap of objects in an image based on Fourier descriptors, with different backbone networks has been proposed in (Upschulte et al., 2022). A dual-path model to identify and fuse low-level and high-level features as the end-to-end network for leukocyte segmentation from blood smear images has been presented in (Dhalla et al., 2023). The encoder block was inspired by the ResNet50 network, and the viral lightweight attention module was focused on spatial and channel features. The transformer-based model in a practical medical scenario of leukocyte detection has been applied in (Leng et al. 2023). In (Depto et al., 2023), medical image imbalance as a crucial issue in the context of predictive modelling was studied in three broad categories: input-based methods, GAN-based methods, and loss-based methods.

Despite recent great advances in supervised learning based medical image segmentation, unsupervised image segmentation remains a promising research direction due to the well-known objectivities of unsupervised learning, especially in the medical field. Unsupervised color image segmentation techniques can be divided into the following categories: thresholding-based methods, edge-based methods, clustering-based methods, region-based methods, graph-based methods, and hybrid methods. Hybrid methods usually fuse different features or combine segmentation results obtained by different methods. However, it is difficult for them to determine the optimal parameters. One of the first applications of artificial neural networks was the development of the pulse coupled neural network (PCNN). The most significant modifications were the RG-PCNN model (Stewart et al., 2002), which combined PCNN with region growing for greyscale image segmentation, and extension of the RG-PCNN model for color images segmentation (Xu et al., 2018).

## 3. MATERIALS AND METHODS

In this section, an overview of the proposed approach is discussed in Section 3.1. Datasets for experiments are briefly described in Section 3.2. The proposed color space correction and CNN-based segmentation are presented in Sections 3.3 and 3.4, respectively.

### 3.1 Overview of the Proposed Approach

Often cell segmentation in blood smear images is performed as a separate mapping for WBCs and RBCs. Due to the fact that WBCs are few number compared to the RBCs ones, methods, first, segment WBCs using pre-processing, color transform, thresholds, and machine learning methods and, second, subtract the WBC map from the initial image in order to segment RBCs. As a result, two maps are obtained. We propose another problem statement that uses the capabilities of CNNs for the semantic segmentation of objects of different sizes and shapes. CNN has encoder-decoder architecture and builds a pseudo-color map. We tested several CNN models using different color spaces converting initial images from RGB to Lab, HSV and CMYK color spaces.

### 3.2 Datasets

For experiments, we used three datasets with varying levels of complexity. The first dataset, CellaVision DM96 (Acevedo et al., 2020), comprises 10,000 images of blood smears captured using a digital microscope. The images have a resolution of 1280×960 and contain different types of blood cells such as red blood cells, white blood cells, platelets, and other artifacts. The dataset is split into a training set of 7,000 images and a test set of 3,000 images, with each image annotated with the type of cell and its location.

The All-IDB dataset (Labati et al., 2011) contains 108 blood smear images with a resolution of 2592×1944 captured at 1000× magnification. The dataset includes both normal and abnormal blood cells, with the abnormal cells classified into different types of leukemia. The dataset is split into a training set of 49 images and a test set of 59 images.

The Blood Cell Detection dataset (Blood Cell Detection Dataset, 2023) is a collection of 12,500 images of blood cells captured under a microscope. The images have a resolution of 640×480 and contain three types of blood cells, namely red blood cells, white blood cells, and platelets. The dataset is split into a training set of 9,375 images and a test set of 3,125 images, with each image annotated with the type of cell and its location. Sample images from these datasets are depicted in Figure 1.

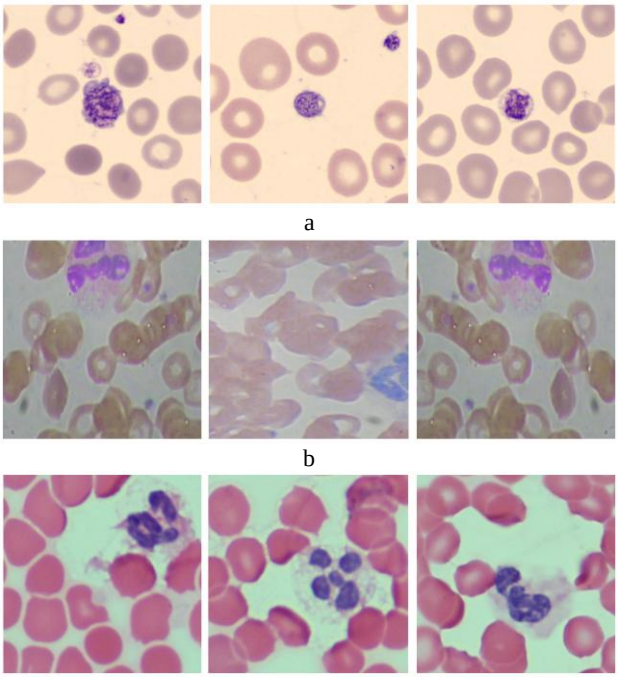

**Figure 1**. Sample images from datasets: a) the CellaVision DM96, b) the All-IDB, c) the Blood Cell Detection.

Preprocessing plays a crucial role in the success of image analysis tasks, particularly in the domain of medical imaging. In this study, we present the preprocessing steps performed on three datasets of blood smear images with varying levels of complexity. Firstly, the images were resized to a fixed size of 256×256 pixels to ensure consistency in the input size of the models. Secondly, color space conversion was carried out from the RGB color space to the Lab, HSV, and CMYK color spaces to experiment with different color spaces. Thirdly, data augmentation techniques, such as rotation, flip, and zoom, were used to increase the diversity of the training dataset and improve the performance of the models. Fourthly, each image annotation was verified by a trained medical professional to identify the regions of interest for the respective cell type (WBCs, RBCs, platelets). Lastly, the annotated images were split into training, validation, and test sets using a random split with a ratio of 80:10:10. In addition, normalization was performed to have a mean of zero and a standard deviation of one, which helps in faster convergence during the training phase. These preprocessing steps ensure the consistency and quality of the datasets, thereby improving the performance of the models during training and testing.

The features of RBC, WBC, and platelets can vary depending on the specific application or analysis being performed. Some common features for each cell type are presented in Table 1.

| Features | RBC | WBC | Platelets |
|---|---|---|---|
| Size | Smaller | Larger | Smallest |
| Shape | Biconcave | Round/Irregular | Oval/Round |
| Color | Red (due to hemoglobin) | Colorless | Colorless |
| Texture | Smooth | Granular | Granular |
| Spatial Distribution | Uniform | Random | Random |

**Table 1**. Some features of RBCs, WBCs, and platelets.

### 3.3 Color Space Correction

In practice, the color of a blood smear image is highly variable due to lighting conditions, different staining times, unstable smear thicknesses, and different physical qualities of samples. In this regard, there is a need for color normalization. One of the simplest approaches is a color correction method based on color transfer between images (Reinhard et al., 2001), one of which is an accurately segmented template image. The color characteristics are transferred from the template to the input image using mean value and standard deviation in Lab color space (Garcia-Lamont et al., 2018). The algorithm includes the following steps:

1. Transform the input image and the template image from RGB color space to Lab color.
2. Calculate the mean value and standard deviation of the input image and the template image in Lab color space.
3. Subtract the mean value from all the pixels of the input image using the following equation:

$$L' = L - \bar{L}\ ;\ \ a' = a - \bar{a};\ \ \ b' = b - \bar{b}\ , \tag{1}$$

where $L, a, b$ = the $L, a, b$ components of each pixel

$\bar{L}$, $\bar{a}$, $\bar{b}$ = the mean values of the $L, a, b$ components

$L', a', b'$ = the resultant values of each pixel

4. Scale the pixels of each color component of the synthesized image, taking into account the corresponding standard deviations:

$$L'' - \frac{\sigma_t^L}{\sigma_i^L} L';\ \ a'' - \frac{\sigma_t^a}{\sigma_i^a} a';\ \ \ b'' - \frac{\sigma_t^b}{\sigma_i^b} b'\ , \tag{2}$$

where $\sigma_t^L$, $\sigma_t^a$, $\sigma_t^b$ = the standard deviation of the $L, a, b$ components of the template image

$\sigma_i^L$, $\sigma_i^a$, $\sigma_i^b$ = the standard deviation of the $L, a, b$ components of the input image

$L'', a'', b''$ = the resultant values of each pixel

5. Transform the synthesized image from the Lab color space to RGB color space.

The application of the algorithm mentioned above helps to better segment WBCs. Example of color transfer is depicted in Figure 2.

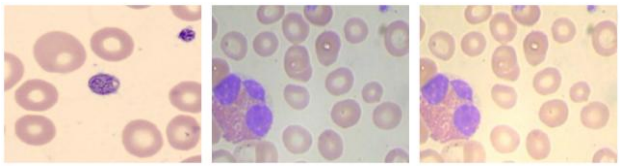

a b c

**Figure 2**. Example of color transfer: a) template image, b) input image, c) synthesized image.

The studies have shown that all types of blood smear cells are visible in three components: the B component of the RGB color space, the V component of the HSV color space, and the Y component of the CMYK color space.

Color space correction is one of the standardisation methods because it can be used to modify the obtained input image to a conventional color characteristic template. Following the color correction phase, the image must be segmented in order to localise the appropriate WBC region. WBC is localised by removing other regions and debris like RBC, platelets, and background. Nevertheless, segmenting the WBC region is difficult due to inconsistent morphological features. This is due to the fact that WBC is divided into two parts: the nucleus and the cytoplasm. The nucleus has higher color intensity than the cytoplasm, and the nucleus is the inner part of the WBC, whereas the cytoplasm is the outer part.

### 3.4 CNN-based Segmentation

To address the aforementioned issues, this study proposed a multi-level deep convolutional encoder-decoder network for blood cell segmentation. An encoder-decoder used to precisely segment WBC particles from blood smear images. It employs CNN-based encoders and decoders that have been pre-trained. As attention maps, the first feature maps built by network are used. These maps are fed into the second network along with the initial 3-channel image to produce the final mask. This mechanism enables the latter encoder-decoder pair to explicitly focus on WBC particles while ignoring other blood cells and debris, improving segmentation accuracy.

In this study, we propose a modified version of the U-Net architecture for the segmentation of blood smear images. The proposed model aims to improve the accuracy of WBC, RBC, and platelet segmentation in blood smear images. The modifications include the addition of batch normalization layers and dropout layers to improve the robustness and generalization of the network. In addition, we incorporated a dilation convolution operation to capture larger spatial context and a squeeze-and-excitation (SE) module to enhance feature representation.

The encoder model consists of four convolution blocks. Each block comprises two convolution layers followed by a batch normalization layer and a ReLU activation function. The convolution layers have a filter size of 3×3 and a stride of 1. Max pooling layers with a filter size of 2×2 are used to downsample the feature maps. Dropout layers with a rate of 0.5 are added after each max pooling layer to prevent overfitting.

The decoder model is composed of four upsampling blocks, each block comprises an upsampling layer followed by two convolution layers with a filter size of 3×3 and a stride of 1. Batch normalization layers and ReLU activation functions are applied after each convolution layer. Skip connections are used to concatenate the corresponding feature maps from the encoder model to the decoder model. In addition, a dilation convolution layer with a dilation rate of 2 is added to capture larger spatial context.

The SE module is added to the decoder model to enhance feature representation. The SE module consists of two fully connected layers with a global average-pooling layer in between. The output of the global average-pooling layer is fed into the fully connected layers with a sigmoid activation function. The modified U-Net architecture is shown in Table 2.

| Layer type | Output size | Filter size/ Stride | Number of parameters |
|---|---|---|---|
| Input | (512, 512, 3) | – | – |
| Convolutional | (512, 512, 32) | 3×3/1 | 896 |
| Batch Norm | (512, 512, 32) | – | 128 |
| ReLU | (512, 512, 32) | – | – |
| Convolutional | (512, 512, 32) | 3×3/1 | 9,248 |
| Batch Norm | (512, 512, 32) | – | 128 |
| ReLU | (512, 512, 32) | – | – |
| Max Pooling | (256, 256, 32) | 2×2 | – |
| Dropout | (256, 256, 32) | – | – |
| Convolutional | (256, 256, 64) | 3×3/1 | 18,496 |
| Batch Norm | (256, 256, 64) | – | 256 |
| ReLU | (256, 256, 64) | – | – |
| Convolutional | (256, 256, 64) | 3×3/1 | 36,928 |
| Batch Norm | (256, 256, 64) | – | 256 |
| ReLU | (256, 256, 64) | – | – |

**Table 2**. The modified U-Net architecture.

The unsupervised deep embedded clustering (DEC) model consists of an encoder, a clustering layer, and a decoder (Xie et al., 2016). The encoder network includes convolutional layers that extract features from the input image. The clustering layer maps the encoded features to a low-dimensional space, where clustering is performed. The decoder network reconstructs the input image from the encoded features. The architecture of the DEC model is presented in Table 3.

| Layer type | Output size | Number of parameters |
|---|---|---|
| Input | (height, width, channels) | 0 |
| Convolutional | (height, width, 32) | 32 |
| Max Pooling | (height/2, width/2, 32) | 0 |
| Convolutional | (height/2, width/2, 64) | 18,496 |
| Max Pooling | (height/4, width/4, 64) | 0 |
| Convolutional | (height/4, width/4, 128) | 73,856 |
| Max Pooling | (height/8, width/8, 128) | 0 |
| Convolutional | (height/8, width/8, 256) | 295,168 |
| Max Pooling | (height/16, width/16, 256) | 0 |
| Convolutional | (height/16, width/16, 512) | 1,180,160 |
| Clustering | (num_clusters) | 524,800 |
| Decoder | (height, width, channels) | 576,576 |
| Total | – | 2,192,192 |

**Table 3**. The DEC architecture.

The DEC model was trained in two phases. In the first phase, the encoder and clustering layers are trained using an unsupervised clustering algorithm such as K-means. In the second phase, the decoder network is trained to reconstruct the input image from the encoded features.

For unsupervised learning, we split the dataset into 80% training data and 20% validation data. We used the binary cross-entropy loss function and the Adam optimizer for training. The learning rate was set to 0.001, and the batch size was set to 16. We trained the model for 100 epochs.

## 4. EXPERIMENTAL RESULTS

In this study, we utilized Python and the Keras deep learning framework to implement our proposed method for blood cell segmentation. The training and testing of the model were performed on a machine equipped with an Intel Core i7 CPU and an NVIDIA GeForce GTX 1080 Ti GPU. Figures 3 and 4 present the accuracy and loss evaluations for the Mod U-net model and the DEC model, respectively.

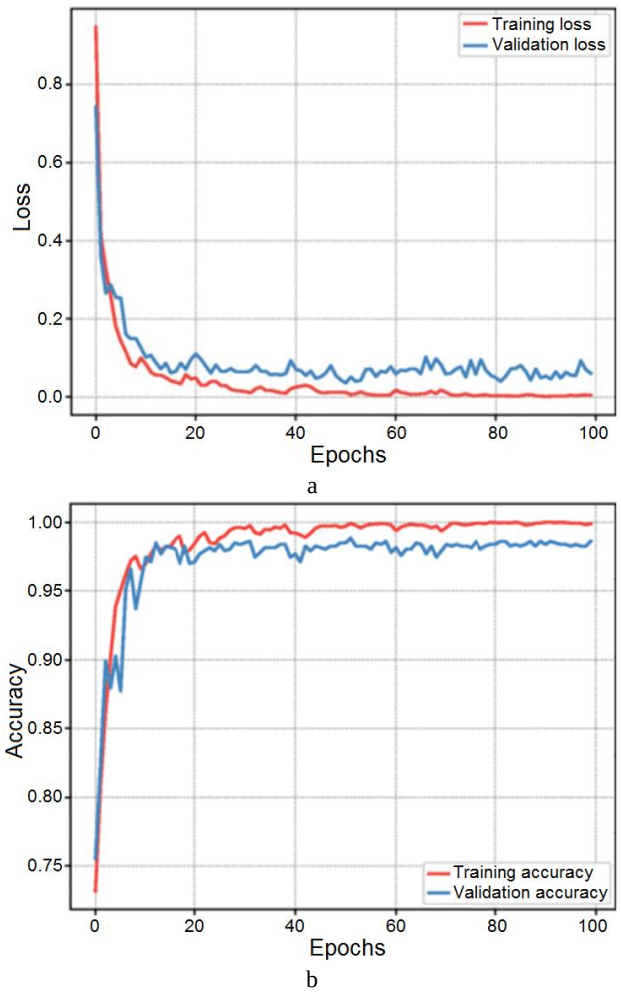


**Figure 3**. Accuracy and loss evaluations: a) accuracy results for the Mod U-Net model, b) losses for the Mod U-Net model.

To evaluate the performance of our models, we utilized several metrics commonly used in image segmentation tasks. Specifically, we reported the precision, recall, and F1-score. The precision metric measures the ratio of true positive predictions to the total number of positive predictions, while recall measures the ratio of true positive predictions to the total number of actual positive cases. The F1-score is the harmonic mean of precision and recall, providing a balanced measure of overall performance. Additionally, we employed the Intersection over Union (IoU) metric, which calculates the ratio of the intersection of the predicted and ground truth masks to their union. Overall, these metrics provided a comprehensive evaluation of the effectiveness of our proposed method for blood cell segmentation. The results of the experiment are shown in Table 4:

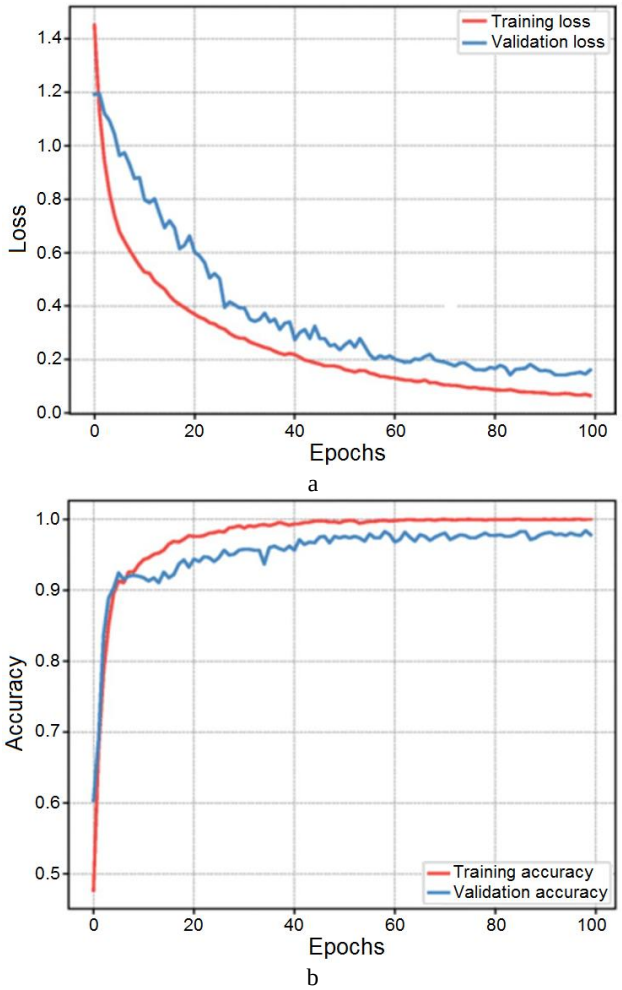


**Figure 4**. Accuracy and loss evaluations: a) accuracy results for the DEC model, b) losses for the DEC model.

| Model | Precision | Recall | F1-score | Accuracy |
|---|---|---|---|---|
| Mod U-Net | 0.94 | 0.97 | 0.93 | 0.93 |
| DEC | 0.84 | 0.89 | 0.86 | 0.81 |

**Table 4**. Average accuracy results of supervised learning (using the modified U-Net model) and unsupervised learning (using the DEC model).

The experimental results of testing our models using different color spaces for blood cell segmentation are summarized in Table 5.

The results show that all color spaces are effective in improving the accuracy, precision, recall, and F1-score of the CNN models for blood cell segmentation. The CMYK color space provides

the highest performance in all models, while the RGB color space provides the lowest performance.

| Model | Color space | Precision | Recall | F1-score | Accuracy |
|---|---|---|---|---|---|
| Mod U-Net | RGB | 0.92 | 0.91 | 0.92 | 0.91 |
| Mod U-Net | Lab | 0.95 | 0.96 | 0.93 | 0.92 |
| Mod U-Net | HSV | 0.94 | 0.92 | 0.92 | 0.92 |
| Mod U-Net | CMYK | 0.96 | 0.96 | 0.94 | 0.94 |
| DEC | RGB | 0.82 | 0.88 | 0.85 | 0.82 |
| DEC | Lab | 0.80 | 0.90 | 0.86 | 0.80 |
| DEC | HSV | 0.80 | 0.87 | 0.89 | 0.81 |
| DEC | CMYK | 0.84 | 0.91 | 0.87 | 0.84 |

**Table 5**. Average accuracy results of supervised learning (using the Mod U-Net model) and unsupervised learning (using the DEC model) depending on color spaces.

The results showed that the use of different color spaces can significantly affect the segmentation accuracy of Mod U-Net models for microscopic images. The best-performing model and color space varied depending on the specific dataset and type of the Mod U-Net model used. This suggests that selecting the appropriate color space for a given task is crucial for achieving accurate segmentation results.

Figure 5 presents the segmentation results for an image taken from the CellaVision DM96 dataset and its different color components using Mod U-net and DEC models. The B component from RGB, the Y component from CMYK, and the V component from HSV were used for experimentation with different color spaces. The red, yellow and blue colors represent RBCs, WBCs, and platelets, respectively.

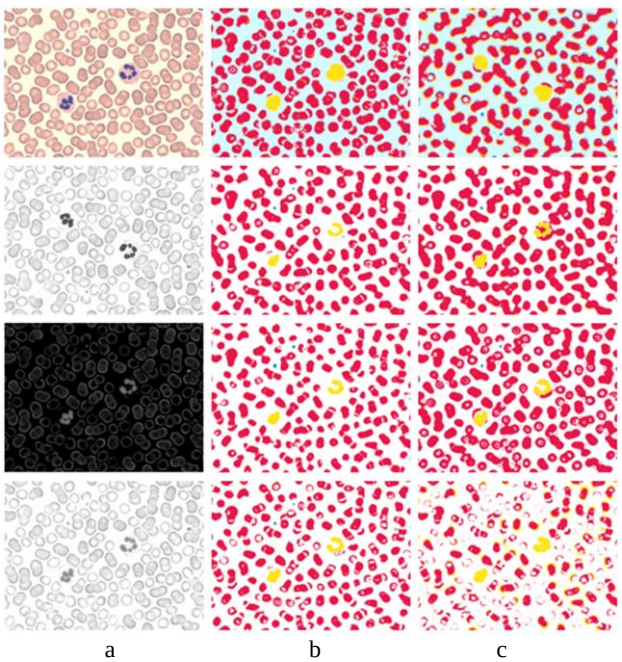

a b c

**Figure 5**. Segmentation results in different color spaces (first row is the RGB representation, second row is the B component from RGB, third row is the Y component from CMYK, fourth row is the V component from HSV): a) input image, b) segmentation using the Mod U-Net model, c) segmentation using the DEC model.

Our approach was evaluated on three publicly available datasets: CellaVision DM96, All-IDB, and Blood Cell Detection. The results demonstrated that our proposed method outperformed the SOTA methods in terms of accuracy and robustness. The U-Net based models achieved an average F1-score of 0.94, IoU of 0.88, precision of 0.94, and recall of 0.95 on the test datasets.

## 5. CONCLUSIONS

We presented a modified approach for blood cell segmentation using deep learning models. We proposed a U-Net based architecture that utilizes residual connections and a combination of convolutional and pooling layers for feature extraction and a series of up-convolutional layers for segmentation. We also experimented with different preprocessing techniques, color spaces, and data augmentation methods to improve the performance of our models. The use of unsupervised clustering algorithms such as K-means for training the encoder and clustering layers of the DEC model has not been so effective.

Overall, our findings suggest that deep learning models can effectively segment blood cells in digital microscopy images, and our proposed approach can achieve high accuracy and robustness in different datasets with varying levels of complexity. Future work can explore the application of our method in other medical imaging tasks and further improve the performance by incorporating more advanced techniques such as attention mechanisms and adversarial training.

## REFERENCES

Acevedo, A., Merino, A., Alférez, S., Molina, A., Boldúa, L., Rodellar, J., 2020: A dataset of microscopic peripheral blood cell images for development of automatic recognition systems. Data in Brief 30. 105474.1-105474.5. doi.org/10.1016/j.dib.2020.105474.

Blood Cell Detection Dataset, 2023: WBC & RBC detection dataset from peripheral blood smears. kaggle.com/datasets/draaslan/blood-cell-detection-dataset (14 February 2023).

Cao, H., Liu, H., Enmin Song, E., 2018: A novel algorithm for segmentation of leukocytes in peripheral blood. *Biomedical Signal Processing and Control* 45, 10-21. doi.org/10.1016/j.bspc.2018.05.010.

Davamani, A.K., Robin R.C.R., Robin, D.D., Anbarasi, J.L., 2022: Adaptive blood cell segmentation and hybrid learning-based blood cell classification: A meta-heuristic-based model. *Biomedical Signal Processing and Control* 75, 103570.1-103570.16. doi.org/10.1016/j.bspc.2022.103570.

Depto, D.S., Rizvee, Md.M., Rahman, A., Zunair, H., Rahman, M.S., Mahdy, M.R.C., 2023: Quantifying imbalanced classification methods for leukemia detection. *Computers in Biology and Medicine* 152, 106372.1-106372.20. doi.org/10.1016/j.compbiomed.2022.106372.

Dhalla, S., Mittal, A., Gupta, S., Kaur, J., Harshit, Kaur, H., 2023: A combination of simple and dilated convolution with attention mechanism in a feature pyramid network to segment leukocytes from blood smear images. *Biomedical Signal Processing and Control* 80, 104344.1-104344.14. doi.org/10.1016/j.bspc.2022.104344.

Drałus, G., Mazur, D., Czmil, A., 2021: Automatic detection and counting of blood cells in smear images using RetinaNet. *Entropy* 23, 1522.1-1522.22. doi.org/10.3390/e23111522.

He, K., Zhang, X., Ren, S., Sun, J., 2016: Deep residual learning for image recognition. *2016 IEEE Conference on Computer Vision and Pattern Recognition (CVPR)*, IEEE, Las Vegas, NV, USA, 27-30 June 2016, pp. 770-778. doi.org/10.1109/CVPR.2016.90.

Garcia-Lamont, F., Cervantes, J., Lopez, A., Rodrigues, L., 2018: Segmentation of images by color features: A survey. *Neurocomputing* 292, 1-27. doi.org/10.1016/j.neucom.2018.01.091.

Guo, Z., Li, X., Huang, H., Guo, N., Li, Q., 2019: Deep learning-based image segmentation on multimodal medical imaging. *IEEE Transactions on Radiation and Plasma Medical Sciences* 3(2), 162-169. doi.org/10.1109/TRPMS.2018.2890359.

Kadry, S., Rajinikanth, V., Taniar, D., Damaševičius, R., Valencia, X.P.B., 2022: Automated segmentation of leukocyte from hematological images – A study using various CNN schemes. *The Journal of Supercomputing* 78(5), 6974-6994. doi.org/10.1007/s11227-021-04125-4.

Labati, R.D., Piuri, V., Scotti, F., 2011: All-IDB: The acute lymphoblastic leukemia image database for image processing. *2011 18th IEEE International Conference on Image Processing (ICIP 2011)*, Brussels, Belgium, 11-14 September 2011, pp. 2045-2048. doi: 10.1109/ICIP.2011.6115881.

Leng, B., Wang, C., Leng, M., Ge, M., Dong, W., 2023: Deep learning detection network for peripheral blood leukocytes based on improved detection transformer. *Biomedical Signal Processing and Control* 82, 104518.1-104518.9. doi.org/10.1016/j.bspc.2022.104518.

Lu, Y., Qin, X., Fan, H., Lai, T., Li, Z., 2021: WBC-Net: A white blood cell segmentation network based on UNet++ and ResNet. *Applied Soft Computing* 101, 107006.1-107006.11. doi.org/10.1016/j.asoc.2020.107006.

Olaf, R., Philipp, F., Thomas, B., 2015: U-Net: convolutional networks for biomedical image segmentation. In: Navab, N., Hornegger, J., Wells, W., Frangi, A. (eds) *Medical Image Computing and Computer-Assisted Intervention – MICCAI 2015*, LNCS, vol. 9351. Springer, Cham, pp. 234-241. doi.org/10.1007/978-3-319-24574-4_28.

Reena, R.M., Ameer, P.M., 2021: Segmentation of leukocyte by semantic segmentation model: A deep learning approach. *Biomedical Signal Processing and Control* 65, 102385.1-102385.13. doi.org/10.1016/j.bspc.2020.102385.

Reinhard, E., Ashikhmin, M., Gooch, B., Peter Shirley, P., 2001: Color transfer between images. *IEEE Computer Graphics and Applications* 21(5), 34-41. doi.org/10.1109/38.946629.

Rodellar, J., Alferez, S., Acevedo, A., Molina, A., Merino, A., 2018: Image processing and machine learning in the morphological analysis of blood cells. *International Journal of Laboratory Hematology* 40(S1), 46-53. doi.org/10.1111/ijlh.12818.

Saraswath, M., Arya, K.V., 2014: Automated microscopic image analysis for leukocytes identification: A survey. *Micron* 65, 20-33. doi.org/10.1016/j.micron.2014.04.001.

Shahzad, M., Umar, A.I., Khan, M.A., Shirazi, S.H., Khan, Z., Yousaf, W., 2020: Robust method for semantic segmentation of whole-slide blood cell microscopic images. *Computational and Mathematical Methods in Medicine* 2020, 4015323.1-4015323.13. doi.org/10.1155/2020/4015323.

Simonyan, K., Zisserman, A., 2015: Very deep convolutional networks for large-scale image recognition. *3rd International Conference on Learning Representations, ICLR 2015*, San Diego, CA, USA, 7-9 May 2015, pp. 1-14.

Stewart, R.D., Fermin, I., Opper, M., 2002: Region growing with pulse-coupled neural networks: an alternative to seeded region growing. *IEEE Transactions on Neural Networks* 13(6), 1557–1662. doi.org/10.1109/TNN.2002.804229.

Tran, T., Kwon, O.-H., Kwon, K.-R., Lee, S.-H., Kang, K.-W., 2018: Blood cell images segmentation using deep learning semantic segmentation. *2018 IEEE International Conference on Electronics and Communication Engineering (ICECE)*, IEEE, Xian, China, 10-12 December 2018, pp. 13-16. doi.org/10.1109/ICECOME.2018.8644754.

Upschulte, E., Harmeling, S., Amunts, K., Dickscheid, T., 2022: Contour proposal networks for biomedical instance segmentation. *Medical Image Analysis* 77, 102371.1-102371.10. doi.org/10.1016/j.media.2022.102371.

Xie, J., Girshick, R., Farhadi, A., 2016: Unsupervised deep embedding for clustering analysis. ICML'16: Proceedings of the 33rd International Conference on International Conference on Machine Learning, vol. 48, New York, NY, USA, 19-24 June 2016, pp. 478-487.

Xu, G., Li, X., Lei, B., Lv, K., 2018: Unsupervised color image segmentation with color-alone feature using region growing pulse coupled neural network. *Neurocomputing* 306, 1-16. doi.org/10.1016/j.neucom.2018.04.010.